# Computational Imaging for VLBI Image Reconstruction

Katherine L. Bouman, Michael D. Johnson, Daniel Zoran, Vincent L. Fish, Sheperd S. Doeleman, and William T. Freeman
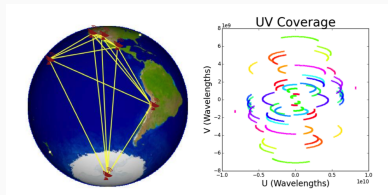
Presented by Elliott Skomski

# Introduction

# Preliminaries

High-res celestial imaging important in astronomy and physics

Global efforts have led to the creation of Event Horizon Telescope

Telescope array emulates a single telescope tens of thousands of km in diameter



Measurements from this telescope array can be used to collect samples with high angular resolution

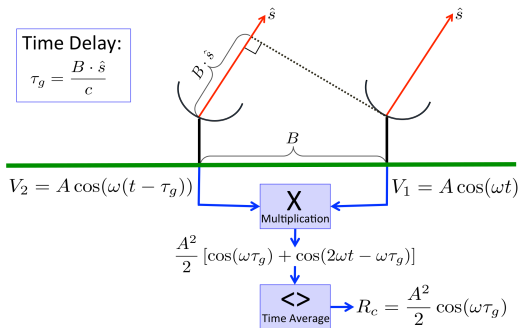Known as very long baseline interferometry (VLBI)

Figure 2. **Simplified Interferometry Diagram:** Light is emitted from a distant source and arrives at the telescopes as a plane wave in the direction $\hat{s}$. An additional distance of $B \cdot \hat{s}$ is necessary for the light to travel to the farther telescope, introducing a time delay between the received signals that varies depending on the source's location in the sky. The time-averaged correlation of these signals is a sinusoidal function related to the location of the source. This insight is generalized to extended emissions in the van Cittert-Zernike Thm. and used to relate the time-averaged correlation to a Fourier component of the emission image in the direction $\hat{s}$.

Even with high-quality measurements, image reconstruction techniques produce poor quality results as resolution increases

Algorithms must depend on fewer measurements

Measurement errors from atmospheric inhomogeneities also become more prevalent

## Proposed Solution

Paper proposes a Bayesian algorithm that models inverse image reconstruction from spatial-frequency measurements

Continuous High-resolution Image Reconstruction using Patch priors (CHIRP)

Makes some simplifying assumptions about atmospheric noise to make the problem more tractable

Paper also introduces a dataset website that allows researchers to access VLBI data

# Methods

# Continuous Image Representation

Reconstructed image $I_\lambda(l, m)$ is defined over continuous space of angular coordinates

Algorithm parameterizes continuous image with discrete number of terms

Allows for the generation of a continuous image, improves reconstruction error

Measured visibility is approximated as Fourier transform of $I_\lambda(l, m)$

This allows image to be parameterized using a discrete number of scaled, shifted pulse functions

Choice of pulse function places implicit prior on reconstruction
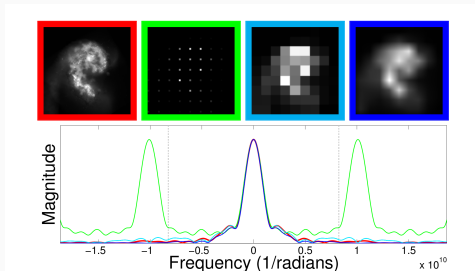


Authors chose a triangle pulse—equivalent to linearly interpolating between pulse centers

Given complex bispectrum measurements $\mathbf{y}$, estimate image coefficients $\mathbf{x}$ by minimizing the energy function:

$$f_r(\mathbf{x}|\mathbf{y}) = -D(\mathbf{y}|\mathbf{x}) - \text{EPLL}_r(\mathbf{x}),$$

where $\text{EPLL}_r$ is the expected log likelihood of a randomly selected image patch

## Data Term $-D(\mathbf{y}|\mathbf{x})$

Image likelihood represented by bispectrum measurements rather than visibility

Data term evaluated for some bispectrum visibility $k$ as

$$\gamma \sum_{i=1}^{M} \left[ \frac{\alpha_k}{2} \left( \begin{array}{c} \xi_k^{\mathfrak{R}}(\mathbf{x}) - \mathbf{y}_k^{\mathfrak{R}} \\ \xi_k^{\mathfrak{J}}(\mathbf{x}) - \mathbf{y}_k^{\mathfrak{J}} \end{array} \right)^T \Sigma_k^{-1} \left( \begin{array}{c} \xi_k^{\mathfrak{R}}(\mathbf{x}) - \mathbf{y}_k^{\mathfrak{R}} \\ \xi_k^{\mathfrak{J}}(\mathbf{x}) - \mathbf{y}_k^{\mathfrak{J}} \end{array} \right) \right],$$

where $\xi_k^{\mathfrak{R}}$ and $\xi_k^{\mathfrak{J}}$ are real and complex terms of ideal bispectrum values extracted from reconstructed image

Gaussian mixture model patch prior used for regularization

We aim to maximize probability of all overlapping pulse patches in reconstruction:

$$\text{EPLL}_r(\mathbf{x}) = \sum_{n=1}^{N} \log p(P_n \mathbf{x})$$

where $p(P_n \mathbf{x})$ is learned through GMM optimization

## Optimization

Energy function minimized using iterative half-quadratic splitting method (Zoran and Weiss, 2011)

To summarize: given set of auxiliary patches $\{z^i\}_1^N$,

- Reformulate cost function as follows:

$$\hat{x} = \operatorname{argmin}_{X \in \Omega} \sum_{n=1}^{n} \left[ \frac{\beta}{2}(||P_n X - z^n||^2) - \log p(z^n) \right]$$

$$+ \sum_{i=1}^{k} \left[ \frac{1}{2} \left( \begin{array}{c} \xi_i^{\mathfrak{R}}(\mathbf{x}) - Y_i^{\mathfrak{R}} \\ \xi_i^{\mathfrak{I}}(\mathbf{x}) - Y_i^{\mathfrak{I}} \end{array} \right)^T \Sigma_i^{-1} \left( \begin{array}{c} \xi_i^{\mathfrak{R}}(\mathbf{x}) - Y_i^{\mathfrak{R}} \\ \xi_i^{\mathfrak{I}}(\mathbf{x}) - Y_i^{\mathfrak{I}} \end{array} \right) \right]$$

- Solve for $\{z^n\}$ given $x$
- Solve for $x$ given $\{z^n\}$

# Results

## Data

At time of writing, EHT measurements were not yet available

Model instead evaluated on synthetic examples and VLBI measurements from VLBA-BU-BLAZAR Program

Synthetic examples include black hole, celestial, and natural images
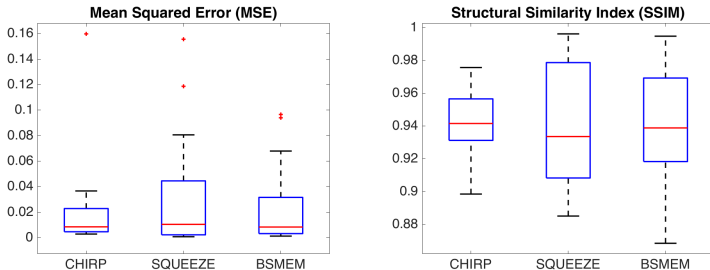
Data publicly available at `vlbiimaging.csail.mit.edu`

Figure 7. **Quantitative Analysis on Blind Test Set:** Box plots of MSE and SSIM for reconstruction methods on the blind dataset presented in Section 5. In SSIM a score of 1 implies perceptual indistinguishability between the ground truth and recovered image. Scores are calculated using the original 'Source' image (Refer to Fig. 4).
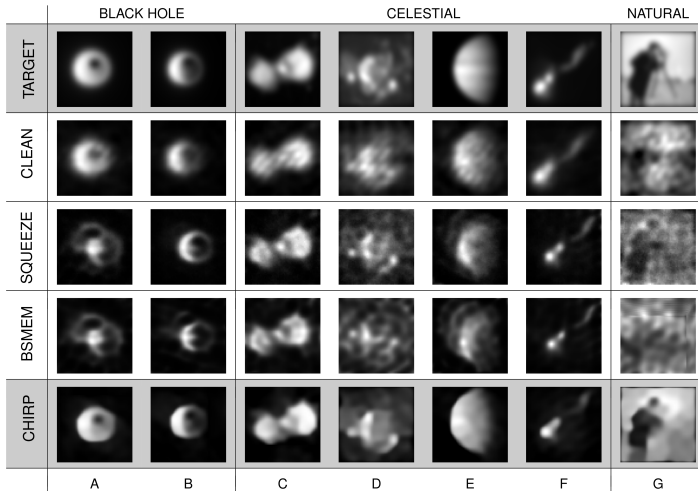
Figure 5. **Method Comparison:** Comparison of our algorithm, 'CHIRP' to three state-of-the-art methods: 'CLEAN', 'SQUEEZE', and 'BSMEM'. We show the normalized reconstruction of a variety of black hole (a-b), celestial (c-f), and natural (g) source images with a total flux density (sum of pixel intensities) of 1 jansky and a 183.82 $\mu$-arcsecond FOV. Since absolute position is lost when using the bispectrum, shifts in the reconstructed source location are expected. The 'TARGET' image shows the ground truth emission filtered to the maximum resolution intrinsic to this telescope array.
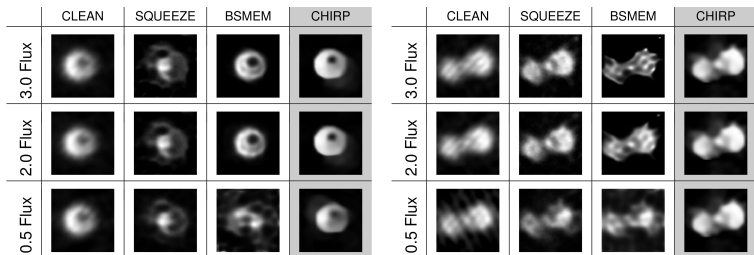
Figure 6. **Noise Sensitivity:** The effect of varying total flux density (in janskys), and thus noise, on each method's recovered reconstructions. Decreasing flux results in higher noise. Notice how our method is fairly robust to the noise, while the results from other methods often vary substantially across the noise levels. The ground truth target images along with the results for a total flux density of 1 jansky can been seen in column A and C of Figure 5.
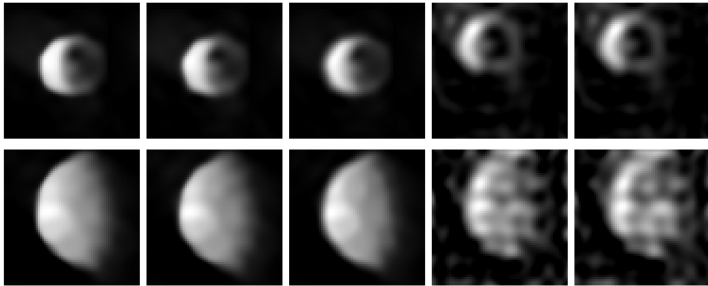
Natural    Celestial    Black Hole    $\ell_2$ Norm    $\ell_{0.8}$ Norm

Figure 8.  **Effect of Patch Prior:** Reconstructions using patch priors trained on natural, celestial, and synthetic black hole images as well as $\ell_2$ and $\ell_{0.8}$ norm priors on the residuals. The ground truth target image are shown in Figure 5 column B and E. The patch priors outperform results obtained using simpler $\ell$-norm priors. Since absolute position is lost during imaging, shifts in the reconstructed source location are expected.
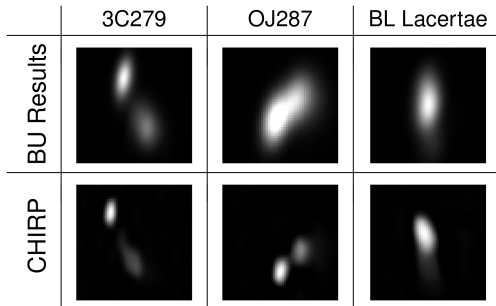
Figure 9. **Real Measurements:** A comparison of our reconstructed images to [23]'s results using CLEAN self-calibration. Note that we are able to reconstruct less blurry images, and are even able to resolve 2 separate, previously unresolved, bright emissions in blazar OJ287. Measurements were taken using the VLBA telescope array. The FOV for each image is 1.5, 1, and 1 milli-arcsecond respectively.

# References

K. L. Bouman, M. D. Johnson, D. Zoran, V. L. Fish, S. S. Doeleman, and W. T. Freeman.
Computational imaging for VLBI image reconstruction: Supplemental material.

K. L. Bouman, M. D. Johnson, D. Zoran, V. L. Fish, S. S. Doeleman, and W. T. Freeman.
Computational imaging for VLBI image reconstruction.
In *Proceedings of the IEEE Conference on Computer Vision and Pattern Recognition*, pages 913–922, 2016.

D. Zoran and Y. Weiss.
From learning models of natural image patches to whole image restoration.
In *2011 International Conference on Computer Vision*, pages 479–486. IEEE, 2011.

Questions?